

JGR Atmospheres

RESEARCH ARTICLE

10.1029/2022JD037696

Key Points:

- Atmospheric electrical conductivity is the key parameter to discern globally representative data (GRD) over the Maitri, Antarctica
- GRD is discernible on a day when conductivity is consistent, and such days are most common in local winter
- In the austral summer, the planetary boundary layer (PBL) processes produce local electrical signals that interfere with the global signals

Correspondence to:

K. Jeeva,
123.jeeva@gmail.com;
jeeva.krishna@iigm.res.in

Citation:

Jeeva, K., Sinha, A. K., Seemala, G. K., Pawar, S. D., Guha, A., Kamra, A. K., et al. (2023). The global representativeness of fair-weather atmospheric electricity parameters from the coastal station Maitri, Antarctica. *Journal of Geophysical Research: Atmospheres*, 128, e2022JD037696. <https://doi.org/10.1029/2022JD037696>

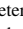





Received 24 AUG 2022

Accepted 17 APR 2023

Author Contributions:

Conceptualization: K. Jeeva
Formal analysis: K. Jeeva
Investigation: K. Jeeva, A. Guha
Methodology: E. R. Williams
Project Administration: A. K. Sinha, Gopi K. Seemala, M. Ravichandran
Resources: M. Ravichandran
Validation: S. D. Pawar
Writing – original draft: K. Jeeva
Writing – review & editing: A. K. Kamra, E. R. Williams

The Global Representativeness of Fair-Weather Atmospheric Electricity Parameters From the Coastal Station Maitri, Antarctica

K. Jeeva¹ , A. K. Sinha² , Gopi K. Seemala³ , S. D. Pawar⁴ , A. Guha⁵, A. K. Kamra⁴ , E. R. Williams⁶ , and M. Ravichandran⁷

¹Equatorial Geophysical Research Laboratory, Indian Institute of Geomagnetism, Tirunelveli, India, ²Department of Physics, School of Science, University of Bahrain, Manama, Bahrain, ³Indian Institute of Geomagnetism, Navi Mumbai, India, ⁴Indian Institute of Tropical Meteorology, Pune, India, ⁵Department of Physics, Tripura University, Suryamaninagar, India, ⁶Department of Civil and Environmental Engineering, Massachusetts Institute of Technology, Cambridge, MA, USA, ⁷Ministry of Earth Sciences, New Delhi, India

Abstract Atmospheric electricity parameters (AEP) measurements from Antarctica predominantly feature either the potential gradient (PG) and/or air-Earth current (AEC) density. We report for the first time simultaneous measurements of the bipolar ions concentration/conductivity, PG, and AEC density. AEP measurements were carried out at Maitri (70.8°S, 11.8°E) from December 2018 to November 2019. We formulated a few criteria, irrespective of the weather conditions, to select the electrically quiet days and some additional criteria based on the conductivity measurements to discern globally representative data (GRD) from such days. The measurements of the PG and AEC density over the Antarctic plateau demonstrated the diurnal curves similar to the Carnegie pattern, which represents the global thunderstorms and electrified shower clouds (ESCs) occurring on different continents and oceans, we regard the data having such trend as GRD. We found significant variability in the concentration of small bipolar ions/conductivity in the austral summer which in turn affects GRD. However, the concentration of bipolar ions is nearly consistent at ~ 250 negative ions cm^{-3} and ~ 300 positive ions cm^{-3} in winter and enhances the probability of GRD. Such differences can arise out of the prevalent planetary boundary layer processes in the two seasons. When the PG varied between ~ 50 Vm^{-1} and ~ 150 Vm^{-1} and the maximum range of conductivity variations was $\sim 0.2 \times 10^{-14}$ C m^{-1} , the AEPs represented the signatures of the global thunderstorm and ESC activities.

Plain Language Summary Monitoring of the atmospheric electricity parameters is a simple technique to monitor global thunderstorm activity and electrified shower clouds. For this, the data need to be free from local disturbances. Obtaining such data in Antarctic Plateau was found to be successful. On the other hand, the coastal Antarctic stations, experience local or regional contributions in it. This paper attempts to provide some techniques to obtain globally representative data (GRD). This paper suggests that the diurnal variation of the concentration of bipolar small ions strongly impacts the GRD. Therefore a day free from the diurnal variation of the concentration of bipolar ions is essential to discern the global signals. The winter season appears to be a better season for this as the summer season experiences mild convection activity that causes local and regional electrical signals that contaminate the data.

1. Introduction

In the study of the global electric circuit (GEC), Antarctica remains a favorite location with the least anthropogenic activity (due to lack of industrialization). Another biggest advantage is that the planetary boundary layer (PBL) processes are the least due to the low elevation of the sun during the summer and its absence above the horizon for a prolonged period in the winter (Cobb, 1977; Deshpande & Kamra, 2001; Reddell et al., 2004). In this context, the Antarctic plateau has proved to be suitable for the potential gradient (PG) and air-Earth current (AEC) measurements owing to their effectiveness in responding to global thunderstorms and electrified shower clouds (ESC) activity (Burns et al., 2005, 2017; Reddell et al., 2004). On the contrary, these measurements in the coastal Antarctic regions are contaminated by locally generated noise caused by sharply varying different meteorological parameters (e.g., Minamoto & Kadokura, 2011). The seasons referred to in the present work are w.r.t. the southern hemisphere.

The winter, spring, and autumn diurnal curves of the PG over Davis (68.5°S, 78°E) (an Australian research station situated in the coastal Antarctic region) show a peak between 1900 UT and 2200 UT. This is similar in both magnitude and behavior to the Carnegie curve which is considered the de-facto standard to evaluate the validity of the attempts to measure universal variations (Burns et al., 1995). The Carnegie curve is a unitary diurnal variation of the PG obtained from 130 fair-weather days of the Carnegie cruise distributed over several years. The majority of them were from Carnegie VII during the years 1928–1929 (Harrison, 2013; Israel, 1973; Whipple & Scrase, 1936). As far as the summer season is concerned, at Davis, the diurnal pattern shows a minor peak between 0300 UT and 1000 UT which is probably due to the local electrical sources. This signature precludes the determination of various external sources such as magnetospheric influences and global thunderstorm features. A recommendation to frame conditions to remove the local contaminations over the global signature was one of the highlights of the study from this location (Burns et al., 1995). A study from Syowa (69.0°S, 39.5°E), a Japanese research station, situated in another part of the coastal Antarctic region, suggests that the data are usually contaminated by local disturbances, thereby, making it difficult to investigate the relationship between the near-earth electric field and upper-atmospheric phenomena (Minamoto & Kadokura, 2011). Another study from Maitri (70.8°S, 11.8°E), an Indian research station situated relatively more interior in the coastal Antarctic region, suggests that there are some anomalous characteristics in the fair-weather PG (Jeeva et al., 2016). This feature is identified from the comparative studies of the PG data at Maitri with that of Vostok and Carnegie curves. While the Carnegie curve and the PG curve at Vostok show a steady increase after 0600 UT, the PG curve at Maitri shows a steady decrease till about local noon. Thereafter PG increases at Maitri, but is not as significant as that at Vostok, thereby, leading to a broad depression in the curve. This, as a consequence, weakens the intensity of the PG caused by the thunderstorms and ESCs over Africa. This behaviour is referred to as the diminished response of the PG to the thunderstorm activity over Africa. The analysis of the PG data from 2005 to 2014 revealed that the diurnal curve obtained from the fair-weather days significantly deviates from the Carnegie pattern by featuring an enhancement in the PG during 0000–0600 UT time domain and a broad minimum between 0800 and 1600 UT. It is also shown that the global characteristics of the PG are dominant in the Austral winter and the anomalous feature is dominant in the Austral summer. However, the contrast in the fair-weather electrical environment in the two seasons was not elaborated on. Tacza et al. (2021) demonstrated the mean seasonal curves of PG for different seasons obtained from the Halley Station, Antarctica. All of them have representations of global thunderstorm activity and ESCs. The significant difference between Halley and the other above-mentioned stations is that Halley is situated on the ice shelf (Brunt Ice shelf). Except for Halley, all the coastal stations mentioned in this study are situated on the open land surface of the continent. This difference will play a crucial role in the absorption of the shortwave solar radiations followed by mild convection observed at the coastal stations over the land surface.

One of the major impediments in the coastal region of Antarctica is that the qualifying fair-weather data is present less than 15% of the year (Burns et al., 1995; Minamoto & Kadokura, 2011). Due to the low percentage of qualifying data, the investigations of the signatures of the global thunderstorms and ESCs, and space weather events over the atmospheric electricity parameters (AEPs), the PG, and AEC, become statistically insignificant. One of the important objectives of the present study is to re-examine the existing set of criteria followed for the fair-weather days, whether it holds at the site of Maitri. We then attempt to define different criteria to select the qualifying data for the global event studies by reducing the severity of the rejection rules for the same.

Usually, diurnal variations of the PG and AEC density have a prominent minimum at 0300 UT followed by a broad maximum that peaks at ~1900 UT (e.g., Carnegie curve). It is believed that these signatures represent the intensity of global thunderstorms and ESCs (Price, 1993). Such a pattern arises due to the difference in the convective activity (an important criterion for thunderstorms and ESCs) when the sun is above the landmass than above the ocean (Price & Rind, 1992). Therefore, the diurnal variations of the PG and AEC density have a close resemblance with these features and are referred to as globally representative data (GRD). However, a deviation in the time and amplitude of the PG and AEC density can happen because of day-to-day variability in the convection activity that governs thunderstorms and ESCs. In the present study, we emphasize the importance of the measurement of the concentration of small ions or electrical conductivity of the atmosphere which are the major contributor to the local electrical disturbances, and their implications in identifying the GRD. We believe that these techniques can be applied in the measurements of AEPs in the rest of the coastal region of Antarctica where the data are usually contaminated by local electrical disturbances. Previous investigators did not monitor the variability of the concentration of small ions (also referred to as air ions) and conductivity. In those reports,

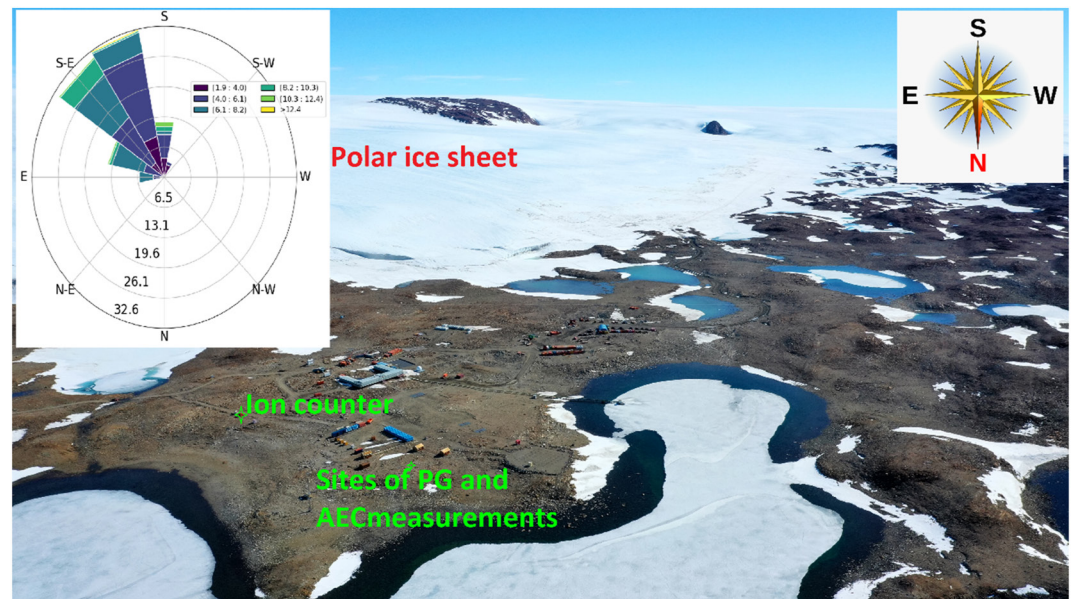


Figure 1. The geographical location of Maitri and the sites of measurement of potential gradient and air-Earth current. The inserted wind rose shows the predominant wind direction on the days free from the circumpolar low-pressure system. The barren land seen in the figure is part of Schirmacher Oasis.

the selection of fair-weather days and selection of the data was mainly based on visual observations such as sky conditions, wind speed, and clouds (Deshpande & Kamra, 2001; Minamoto & Kadokura, 2011; Ruhnke, 1962). This method is lacking in identifying the invisible electrical perturbations that would suppress the GRD.

2. Description of the Experiment Site and Its Climate

Figure 1 shows the location of Maitri (70.8°S, 11.8°E, +117 m) and different sites wherein the observations of the AEPs were done. A wind rose diagram is presented in the inset in Figure 1 to show the predominant wind direction on fair-weather days for 2019 (the period of study). Maitri station is located in Eastern Antarctica in the region of Queen Maud Land (between 0° and 30°E) on the Schirmacher Oasis with an open landmass area of ~18 km × 3 km elongated in the east-west direction. This open area is partly covered by snow from March to November in a typical year. The station is surrounded by a polar ice sheet on the south side. There are low-lying hills of different altitudes up to ~130 m present on the northern side. Beyond the hills, ~80 km stretch of shelf ice connects the mainland and the ocean. Since the longitude is close to the Greenwich meridian (~11°E) the 44 min difference between the UT and LT is generally insignificant in the present study.

The Schirmacher Oasis has 118 lakes with different freshwater sources. They are classified as periglacial, proglacial, and epishelf lakes (Ravindra et al., 2004). These lakes are in a frozen state except during the peak of Austral summer (December to February). Patches of soft snow are prevalent during the months of March–November due to precipitation associated with circumpolar storms. The melting process is associated with varying air temperatures, solar radiation, snowmelt, wind, precipitation, etc., (Dirscherl et al., 2021). The Antarctic continent is known for its vast and thick ice sheet covering ~98% of the landmass. This provides a unique characteristic of the continent to prevent the atmosphere to have direct contact with the surface of the continent. This will suppress the emanation of radioactivity released into the atmosphere and PBL processes caused by the absorption of incoming solar radiations and resulting convection. Nevertheless, the remaining 2% of the Antarctic continent is exposed to the atmosphere. This surface is subject to mild heating during the summer season.

Atmospheric depressions are more frequent in the Coastal Antarctic region than in the interior part of the continent (King & Turner, 1997). Maitri is strongly influenced by the eastward-moving depressions which encircle the continent between 60°S and 65°S. This system is the major source of moist air and deposition of snow over the coastal Antarctic region. We excluded the days influenced by the low-pressure system to understand the mean weather and climate. It is well known that the movement of extra-tropical low-pressure systems can push warm and moist air over the coastal Antarctic region. On such days, weather parameters can strongly deviate from their

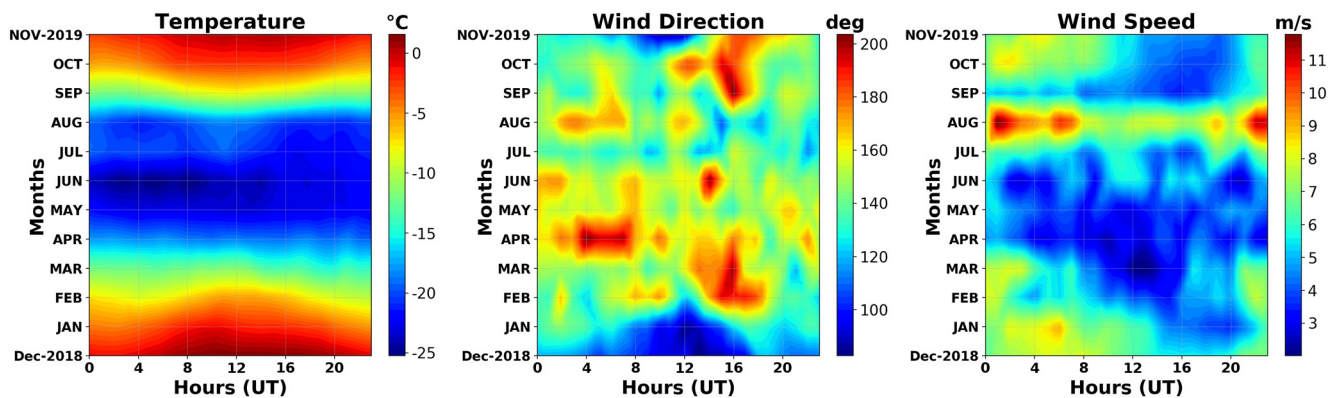


Figure 2. The monthly mean diurnal variation of the (a) temperature, (b) wind direction, and (c) wind speed at Maitri.

mean value (Ramesh & Soni, 2018). We, thus, had 110 days of data that were free from the influence of the low-pressure system during the period December 2018 to November 2019, for further study/to study the climate for the period. Figure 2 shows the monthly mean diurnal variation of the surface air temperature, wind direction, and wind speed. The surface air temperature experiences a maximum (between 0°C and 5°C) in December and January. This is due to solar energy warming up the Earth's surface to produce weak thermal convection during these months (Gajananda et al., 2004; Naithani & Dutta, 1995). The temperature shows a decreasing trend from the beginning of February onwards. Usually, the minimum temperature is recorded either in August or September. The average mean minimum temperature was observed to be $\sim -25^{\circ}\text{C}$ (Figure 2a). As far as the time dependency of the direction of the wind was concerned during night hours the wind is from ESE and SE. It gradually shifts from SE to the east by 1400 UT (Figure 2b). The wind speed maximizes at ~ 0000 UT. Thereafter, it gradually decreases to attain its minimum at ~ 1600 UT followed by an increase to attain its maximum again at midnight hours (Figure 2c). The katabatic wind is defined as the flow of cold and dense air along the downslope under the influence of gravity (Lutgens & Tarbuck, 2001). The slope of the ice sheet is in the southeast quadrant (Kumar et al., 2007). Therefore the winds reported here could be katabatic.

3. Instrumentation and Theory

3.1. Electric Field Monitor and Electrometer

The electric field monitor (EFM) is made by Boltek Corporation, Canada and the model is the EFM-100. It is a commonly used instrument for the measurement of the fair-weather electric field. Out of 17 sites in the Global Coordination of Atmospheric Electricity Measurement (GloCAEM), this Boltek EFM-100 is used at seven sites (Nicoll et al., 2019). The sensitivity of the EFM is 1 V/kV in dual-output mode and 0.5 V/kV in single-ended output. In remote locations, the stepped-range voltage technique is applied to standardize the unit of the PG. More technical information is provided by Jeeva et al. (2016, 2021).

Different types of antennas are used to sense the AEC and are elaborated on by Jeeva et al. (2021). In the present study, the current sensed by a 10 m long-wire antenna is used. The current signal from the antenna is fed to an electrometer (Model AD 549) that has high input impedance and permits an extremely low input bias current (10^{-14} A). The electrometer measures the current up to 1 nA (corresponding to the output voltages whose limit is ± 5 V) with a feedback resistance of 5×10^9 . A unity gain operational amplifier (LM308) amplifies the electrometer output signal. The amplified signal, using LM 308, is carried by a shielded cable over a distance of 10 m to the observatory to be logged on a PC-based data logger. The time constant of the electrometer is maintained at $\sim 1,000$ s which is nearly equal to the relaxation time of the GEC (Burns et al., 2012). Jeeva et al. (2021) measured the current density with different R-C time constants in different electrometers. The results from all the electrometers showed a similar result. The sensitivity of the digitized signal is 2.44 mV which corresponds to a current of 0.5 pA. Both, the PG and the AEC are sampled at the rate of 1 s.

3.2. Bipolar Conductivity and Concentration of Bipolar Small Ions

Gerdien condensers and ion counters are used to monitor the atmospheric electrical conductivity and bipolar small ion density respectively. While the Gerdien condensers are installed outdoors at an altitude of 0.5 m from

the Earth's surface the ion counter is installed at a height of 1 m in a semi-outdoor position that is, the ion counter is installed inside a laboratory hut but the air from the atmosphere is drawn by the suction fans into the counter. This arrangement is preferred to protect the electronic console which contains a Liquid Crystal Display (LCD) and which cannot function in the sub-zero temperature. The design of the Gerdien condensers is based on Dhanorkar et al. (1989). It is a cylindrical-shaped condenser with an outer electrode and a coaxial inner electrode. It is a successful apparatus design and employed in various studies in the past (Jeeva et al., 2011; Nagaraja et al., 2003). A pair of condensers are connected by a U-shaped tube to make it a single unit where the aspiration fan is fixed at the end of the U-tube as a common source of air aspiration. The dimensions of both the electrodes, the biasing voltage, and the speed of air in the condensers are suitably adjusted so as to detect all the small ions in the sucked air having mobility $>0.70 \times 10^{-4} \text{m}^2 \text{V}^{-1} \text{s}^{-1}$. It can measure the conductivity of air as low as $3 \times 10^{-16} \text{ } \Omega \text{ m}^{-1}$. The ionic current is then fed to two separate electrometers (AD 549) and data are sampled using a National Instruments data logger every 1 s. The final conductivity is derived from the following equation given by Mac Gorman and Rust (1998):

$$\sigma_{\pm} = \epsilon_0 i / CV \pm \quad (1)$$

where ϵ_0 is the permittivity of the air ($8.85 \times 10^{-12} \text{ Fm}^{-1}$), i is the ionic current, C is the capacitance of the apparatus (viz. 24 pF) and V is the applied voltage.

3.3. Ion Counter

We utilize an ion counter manufactured by Com System Inc., Japan (Model: COM-3800 V2) which is widely used to monitor the concentration of bipolar air ions (in the range of 0–5 106 ions cm^{-3}) with an accuracy of $\pm 10\%$ (Wang et al., 2020). It works on the well-known principle of the Gerdien condenser which is explained in Section 3.1. It can measure the ions that have mobility $\sim 0.70 \times 10^{-4} \text{ m}^2 \text{v}^{-1} \text{ s}^{-1}$ with an accuracy of 10%. Similar to Gerdien condenser measurements, the data are sampled every second. We compare the conductivity measured by this condenser with that obtained from the ion counter. The conductivity using the ion counter is calculated using the following well-known equation:

$$\sigma_T = n_T \mu e. \quad (2)$$

where σ_T is total conductivity, n_T is the total ion density ($n_- + n_+$), μ is the mobility and e is the electron charge ($1.6e^{-19} \text{ C}$). Our ion counter detects the small ions having $\mu = 0.7 \times 10^{-4} \text{ m}^2 \text{V}^{-1} \text{ S}^{-1}$.

4. Observations and Results

4.1. Ion Counter, Gerdien Condenser Measurements, and Their Comparison

Figure 3 presents typical examples of the ion counter measurements carried out at Maitri. The left, middle, and right columns of Figure 3, respectively, show the diurnal variation of measurements carried out on 19, 20, and 21 January 2019. We have selected these days to highlight the nature of diurnal variation on three consecutive days as well as to ensure the satisfactory functioning of the ion counter at par with the extensively used Gerdien condensers. The upper row presents the concentration of bipolar ions and the middle one shows the bipolar conductivity measured using the Gerdien condenser. A comparison of the conductivity measured using the Gerdien condenser is shown in the middle and that derived from the ion counter measurements is presented in the bottommost row. We observed that the conductivity measured using the Gerdien condenser is ~ 3 times higher than that of the calculated one from the ion counter measurements. We believe that this difference could probably be due to the difference in their installation locations and instrument tolerance. Because one system (Gerdien condensers) was installed 0.5 m above the earth's surface in the open space and the other system (ion counter) was installed semi-indoors (wherein the system is indoors but the air is sucked into the ion counter directly without any tube or conduits from the free space) at 1.2 m above the earth's surface. An attempt was made, at a later stage, to examine whether there is a difference in the concentration of ions observed from semi-indoor and outdoors.

Figure 4 shows the comparison of the simultaneously monitored concentration of bipolar air ions on 25 January 2022. Figure 4a depicts the diurnal variation of the bipolar air ions observed semi-indoor and Figure 4b shows the same but for out-door. The comparison reveals that the diurnal patterns of concentration of negative ions correlate with $R = 0.8$ and positive ions with $R = 0.1$. The variation of the concentrations in the semi-indoor appears to

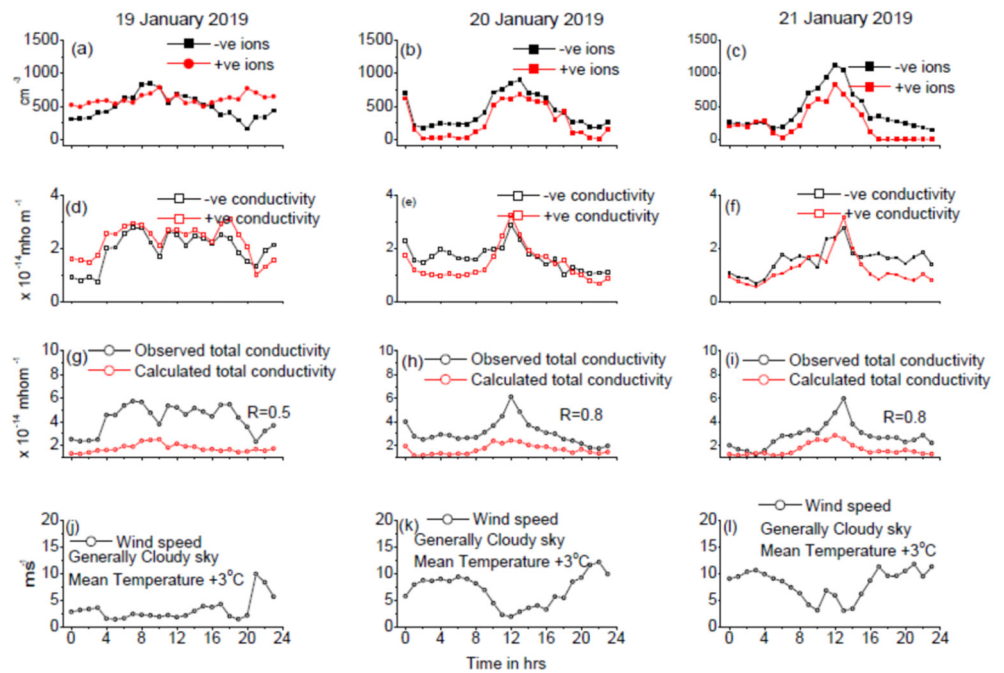


Figure 3. (a)–(c) Diurnal variation of the concentration of bipolar small ions observed by the ion counter on 19, 20, and 21 January 2019. (d)–(f) Diurnal variation of the bipolar conductivity measured by Gerdien condensers on these days. (g)–(i) Comparison of the conductivity obtained by Gerdien condensers and that estimated from the ion counter measurements. The correlation coefficient between the two measurements is also shown. (j)–(l) observed wind speed on the respective days.

be damped. The concentration of negative ions on semi-indoor is 40% less than outdoors. Whereas, the negative ion concentration at semi-indoor is 14% less than at the outdoor position. Some of these features invite a detailed study which is in progress to deal with these issues. Two measurements show an impressive correlation on 20 and 21 January 2019. While this is slightly lower (~ 0.5) on 19 January which can be due to a mild enhancement in the concentration of positive ions in contrast to that of negative ions during 1500–2400 UT. In general, the two measurements greatly co-vary with the correlation coefficient ranging between 0.5 and 0.8. On 19 January 2019, the significant difference in the weather was that the wind speed was $\sim 3 \text{ ms}^{-1}$ throughout the day except after 2000 UT. There was no diurnal variation. On the other hand, the remaining 2 days showed a significant level of diurnal variation with a broad minimum during the daytime. The concentration of ions is maximum when the wind is minimum (at noon hours) and, it is minimum when the wind speed is maximum (during night hours). It implies

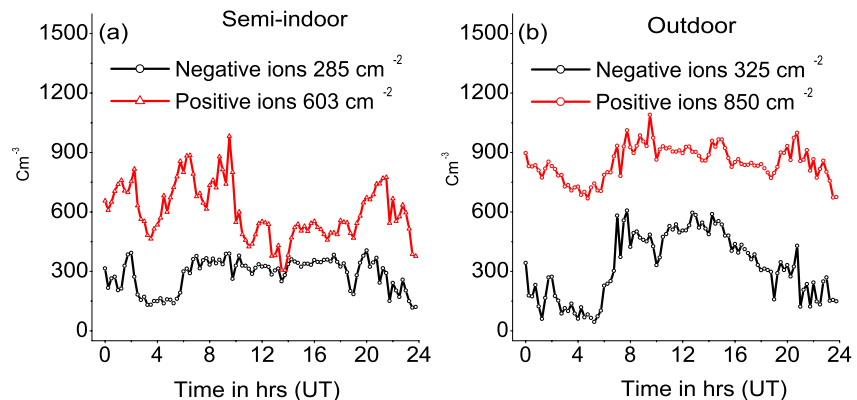


Figure 4. Comparison of the concentration of simultaneously measured air ions in (a) Semi-indoor and (b) outdoor positions of two ion counters. The diurnal patterns of the concentration of air ions observed at both positions are nearly similar for the negative ions but not for positive ions. The magnitude of concentration for outdoor measurement is higher than the semi-indoor. This is 40% for negative ions and 14% for positive ions.

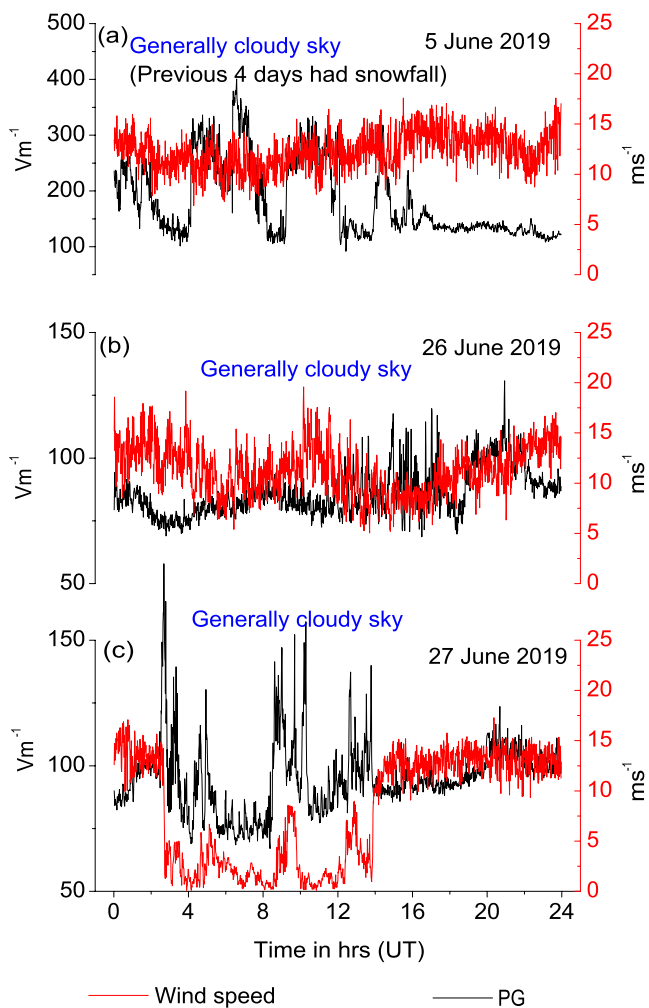


Figure 5. Diurnal variation of 1 min averaged potential gradient observed at Maitri on 5, 26, and 27 June 2019 (a), (b), and (c) respectively. The rapid variation observed on 5 June 2019 suggests that there is strong charge separation due to different processes other than the DC global electric circuit variations. Such days are discarded from the analysis of the fair-weather electric environment. On 27 June 2019, (c), there is a moderate fluctuation during the UT hours 0200–0500, 0800–1100, and 1200–1400. The data points relevant to such a disturbed period are removed. And the remainder of the data is considered for analysis. On 26 June 2019 (b), there is no rapid fluctuation and this day is the best example of a day free from charge separation.

not been considered but the remainder is used in our analysis. On 26 June 2019, the PG variations were almost free from the above-mentioned rapid fluctuations and have been considered for further study. Rapid fluctuations are primarily driven by the short period of local weather disturbances which can have a time scale ranging from a few seconds to a few minutes. An hourly-averaged data may not address these effects and therefore, we have considered 1-min averaged data for data rejection. An elaborative account of such a choice is presented in the Discussion section in terms of atmospheric relaxation time.

We applied these standards to filter out contaminated data when precipitation, blowing snow, drifting snow, and strong, low clouds occurred and selected 15 days of quality data for further study in March 2019. We were motivated by the fact that a variety of sky conditions and wind speeds prevailed during this month which provided us an opportunity to test the effectiveness of these criteria. We present the diurnal variation of hourly averaged data of the PG in Figure 6 for these days. The averaged diurnal variation of the PG of the same is also shown at

that the ions produced during calm wind conditions are dispersed by the wind when its speed is increased (perhaps beyond $\sim 8 \text{ ms}^{-1}$). This is evident from the data on 19 January 2019. At 2100 UT the wind speed has increased from 2 to 10 ms^{-1} . The conductivity and the concentration of negative ions have sharply decreased. Therefore the mechanisms involved in the production and loss of air ions, particularly the excess negative ions, are being addressed through (a) the Lenard effect (Lenard, 1892), (b) the Electrostatic interface (Dinger and Gunn (1946) in a separate study.

4.2. Selection Criteria and Qualifying Data: An Overview

Identifying suitable PG or AEC density data for the investigation of the global feature is usually done by applying some rejection criterion which is based on the visual observation of the sky condition (i.e., visibility), and the limiting threshold for wind speed, etc., (Deshpande & Kamra, 2001; Minamoto & Kadokura, 2011; Ruhnke, 1962). The global features are well represented/ detected in the PG and AEC density variations in Antarctic Plateau (Bering et al., 1991; Burns et al., 1995, 2017; Byrne et al., 1993; Cobb, 1977; Frank-Kamenetsky et al., 2001; Jeeva et al., 2016). However, these variations also show strong signatures of local electrical disturbances in coastal Antarctica (Burns et al., 1995; Jeeva et al., 2016; Minamoto & Kadokura, 2011). Thus, the usefulness of these selection criteria of GRD over these sites needs to be reviewed. As an example, Jeeva et al. (2016) carried out the GEC experiments at Maitri for about 6 years spread during 2006–2020. The lead author found that the strong winds associated with the snow particles, snowfall, and drifting snow caused severe fluctuation in the PG and AEC density variations, during his stay in Antarctica. Also, distorted diurnal patterns were seen during the presence of low clouds. Under these circumstances, Burns et al. (2012) set an upper limit of PG to 350 Vm^{-1} and rejected the data before 2 hr when the PG exceeded this limit and until 2 hr after it returned below 350 Vm^{-1} . Jeeva et al. (2016) found that this rejection criterion works well at Maitri for the data contaminated with the above-mentioned factors and a typical example is presented in Figure 5. Figure 5 shows a 1-min averaged diurnal variation of the PG for 5, 26, and 27 June 2019. On 5 June, the PG variation (shown in blue line with symbol) showed unusual fluctuations during 0400–1600 UT and reached up to $\sim 400 \text{ Vm}^{-1}$. A rapid jump of PG to $\sim 400 \text{ Vm}^{-1}$ is seen at 0600 UT and we rejected data from 0400 to 0800 UT following Burns et al. (2012). Again, “rapid and large fluctuations” were seen not on par with fair-weather days during ~ 0900 –1500 UT. We believe that the remaining data might have some influence on local disturbances seen prior and so have rejected this day for further analysis. On 27 June 2019, the PG data (shown in the red curve) experienced unusual fluctuations for short periods during 0300–0500 UT and 0900–1100 UT. Such disturbed data have

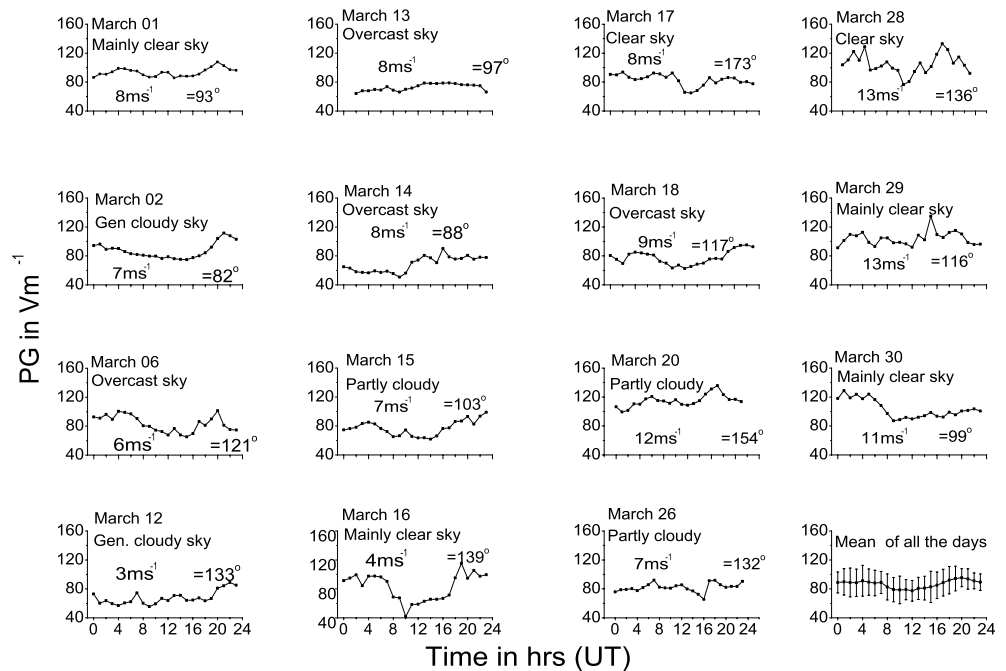


Figure 6. Diurnal variation of hourly averaged data of the potential gradient for 15 qualifying days in March 2019. The sky condition and daily mean wind speed (v) and mean wind direction in (φ) of each day are labeled in each panel. The common feature observed on all the days is a pre-midnight peak except for a couple of days on 26, and 27 March 2019.

the rightmost panel of the bottom row. It is evident that the mean curve does not represent the expected global minimum of ~ 0300 UT. Instead, it shows a mild peak around this time and a broad depression centered the noon. This is a typical Type 3 variation reported by Jeeva et al. (2016). The Type 3 variation is the hourly mean diurnal variation of PG showing a broad minimum centered at 1200 UT that makes the PG diurnal pattern strongly deviate from the UT-dependent variation. Therefore it is inferred that the data selected based on the aforesaid criteria provide a smooth diurnal curve but does not appear to bear the signatures of the GRD. One of the prominent features, the minimum at ~ 0300 UT is absent as well as the shape of the curve is different from the UT curve of the PG. It is seen that the electrically quiet days demonstrate different diurnal trends. At this stage, it is difficult to identify the GRD. Because the shape of the diurnal curve alone does not guarantee the GRD as there can be day-to-day variability in the globally distributed thunderstorm and ESCs. However, we followed the following criteria to identify the qualifying data for the present study;

- (i) One-minute averaged data is suitable to discard the undesirable data rather than the hourly data.
- (ii) A day having strong and rapid fluctuations, exceeding 350 Vm^{-1} , for more than half of a day is rejected. These days are referred very noisy days (5 June 2019 in Figure 5).
- (iii) A day having a $\sim 20\%$ increase or decrease in the value of the PG or AEC density between two successive points or, for a short period, approximately 4 hr in a day, is referred to moderately noisy day (27 June 2019). The data from these days are considered after rejecting the data pertaining to the period of rapid fluctuations as well as 2 hr prior and later to the disturbed period. If the moderately noisy period continues for more than half of a day this day is also rejected.
- (iv) A day having smooth variation, a data point having less than 20% increase or decrease in the successive value, is referred to electrically quiet day (26 June 2019, Figure 5).

4.3. Seasonal Variations of PG, AEC Density, and Concentration of Air Ions

Jeeva et al. (2016) studied the seasonal variation of the PG and found that the austral winter season is the suitable season for the GRD of the PG and AEC density and the austral summer bears anomalous characteristics; however, did not then account for such behavior. We attempt to address this issue in support of the concentration of bipolar small ions (a proxy for the electrical environment) and weather parameters during two contrasting seasons viz. the

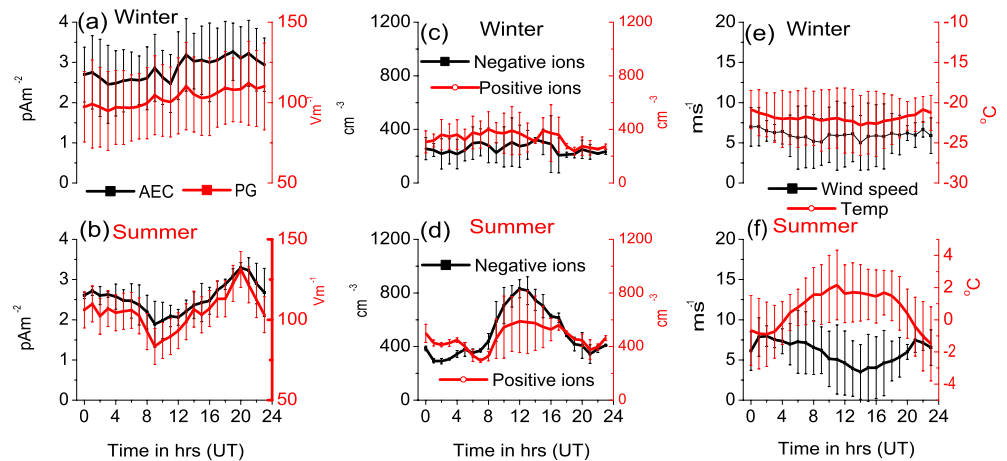


Figure 7. Fair-weather diurnal mean curves of various atmospheric electricity parameters and meteorological weather parameters during the winter of 2019 (June–July (7 days)) and the summer of 2018–2019 (December–January (13 days)). (a), (b) potential gradient and air–Earth current density for winter and summer, respectively. (c), (d) Concentration of negative ions and positive small ions for winter and summer, respectively. (e) Temperature and wind speed for winter and summer, respectively.

austral winter and summer. We utilized data from 13 fair-weather days June–July 2019 to determine the diurnal trend in winter. Similarly, we used 17 fair-weather days from December 2018 to January 2019 to derive the trend in summer. We have selected these days based on the criteria presented in this paper in the section conclusion.

Diurnal curves of the PG and the AEC density in winter in Figure 7a show a clear minimum at 0300 UT followed by a steady increase thereby attaining a maximum at ~1900 UT. Such a trend represents the general diurnal behavior driven by global thunderstorm activity and ESCs. On the other hand, both PG and AEC density variations in summer in, Figure 7b, resemble the anomalous pattern of the PG at Maitri reported by Jeeva et al. (2016). The diurnal variation of the concentration of negative and positive ions in Figure 7c shows a flat response centered on $\sim 250 (\pm 36) \text{ cm}^{-3}$ and $335 (\pm 49) \text{ cm}^{-3}$, respectively. In contrast, both these parameters show large variability from $\sim 400 \text{ cm}^{-3}$ to 3 (during the night-time) to $\sim 800 \text{ cm}^{-3}$ (in the daytime) in summer (Figure 7d). We observed an interesting behavior during 0000–0400 UT and 1900–2300 UT wherein positive ions dominate over the negative ions, and vice versa during 0600–1800 UT. This suggests an additional production mechanism of one type (unipolar) of ion during the period of interest. So far as their diurnal variation is concerned, both ions show a peak density at $\sim 1200 \text{ UT}$. Negative ions showed a sharp maximum; however, the positive ions showed a broad maximum. As will be seen later, the diurnal behavior of negative ions appears to be more sensitive to temperature than the positive ions. The physical process of this event shall be studied separately in the future.

4.4. Proposed New Criteria for the GRD

Based on the long-term measurements of the PG over Vostok, Burns et al. (2012) put forward a set of criteria for data selection that successfully addressed/detected the global features therein. Upon following these criteria, Jeeva et al. (2016) found that the PG data set in general contained anomalous variations caused by local influences rather than the GRD. A similar situation is observed in the present study. Figure 7 suggests that the PG and AEC density data represent the global features better in winter than in summer. We found the conductivity to be substantially more stable throughout 24 hr in winter. Motivated by this, we attempted to understand if the range of variability of conductivity could be taken as an additional selection criterion. We identified a few days on which the total conductivity is nearly free from the diurnal variations. They are 11, 13, 25, 26, 28, 29, and 30 July 2019. On these days the total conductivity (viz. the sum of the conductivity due to both positive and negative ions) varied between 0.2×10^{-14} and $0.8 \times 10^{-14} \text{ } \Omega \text{ m}^{-1}$, irrespective of the sky and general weather conditions. Therefore it is inferred that the range of the total conductivity mentioned above can be considered as a threshold to claim the atmosphere is electrically stable. We estimated the mean PG and AEC density using these data, as shown in Figures 8a and 8b, respectively. Also shown in Figure 8b is the AEC density calculated using Ohm's law relation $j = \sigma E$. Figures 8c and 8d, respectively, show the mean total conductivity and the correlation coefficient between the observed and calculated AEC density.

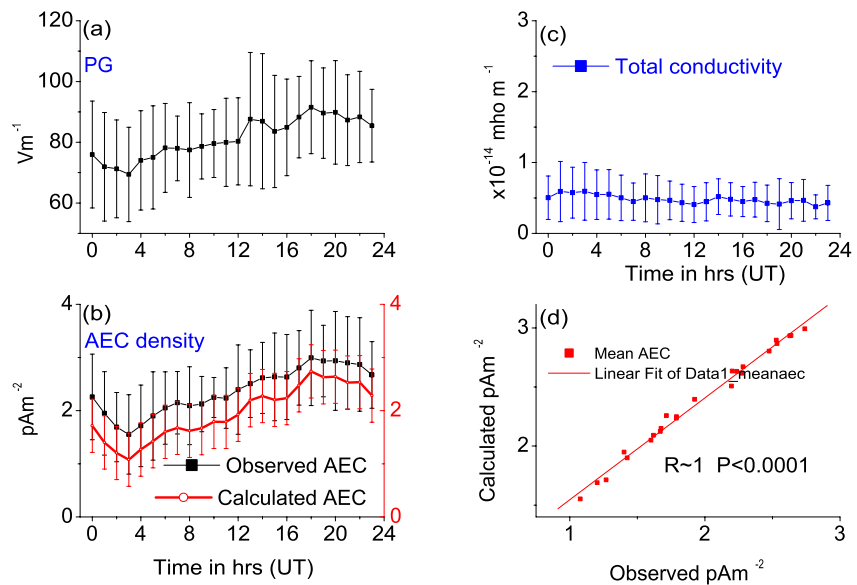


Figure 8. (a) Diurnal variations of potential gradient (PG) in winter derived using the total conductivity as an additional selection criterion of globally representative data. The mean of 7 days of data on 11, 13, 25, 26, 28, 29, and 30 July 2019 has been presented. (b) Same as (a) but for observed air-Earth current (AEC) density (black curve), and that of calculated one using the relation $j = \sigma E$ (red curve) (c) Mean total conductivity. PG and AEC density variations show a prominent peak at 1800 UT (corresponding to thunderstorm/lightning activity over the Americas) and two shallow peaks at 0700 UT and 1400 UT (the usual signatures of global thunderstorm and electrified shower cloud activity over Asia and Africa, respectively) (d) Scatter plot of observed and calculated AEC density.

Next, we attempt to study the effectiveness of this conductivity criterion in the summer. We observed earlier that the concentration of small ions, in summer, shows a maximum at noon and a minimum at night hours (see Figures 3 and 7). However, the conductivity shows a plain response on some occasions particularly when there is a mild breeze. We selected 12 qualifying days of data in January 2019 and grouped them into two. Group 1 consisted of data on 1, 2, 16, 18, and 19 January 2019 when the conductivity showed greater stability. Another set of data, Group 2, featured data on 3, 4, 5, 6, 15, 20, 21, and 22 January 2019 when strong diurnal variability of the conductivity was seen. Figure 9a shows the mean diurnal variation of the total conductivity for Group 1 day Figure 9b shows the observed (black line with symbol) and calculated (red line with symbol) AEC density. Figure 9c shows the mean diurnal variation of the PG for the Group 1 day. The same parameters are shown on the right side column of Figure 9 but for Group 2 days. We found a high correlation coefficient of ~ 0.8 between the observed and calculated AEC density for Group 1; however, a poor correlation of 0.2 is seen for Group 2 days. When there is consistency in the electrical conductivity throughout the day, an excellent agreement is seen between observed and calculated AEC density. In contrast, this is not seen when the conductivity has a strong diurnal variation (Figure 9d). The mean standard deviation for Group 1 is 0.07 and for Group 2 it is 0.7.

5. Discussions

5.1. On Sampling Interval of 1 Min Averaged Data

To understand the influence of local weather disturbances in defining the qualifying data, we have considered 1-min averaged data for data rejection. Such a choice follows from the fact that the atmospheric-electric time constant is an important aspect of the study of GEC. It is the time in which a steady-state condition is restored after a significant change in the atmospheric electric condition. According to Chalmers (1957), it is between 5 and 40 min; Israel (1957, 1970) calculated it to be 30 min. Therefore, either 30-min average or 1-hr data opted in the study of the diurnal or seasonal variation of the PG and AEC density. Short-period fluctuations of less than 30 min can probably arise due to the electrical perturbation close to the surface level. Therefore, such contaminated data need to be rejected. This cannot be achieved in the hourly mean data. Thus, we fix the criterion for the data selection based on the 1-min averaged data.

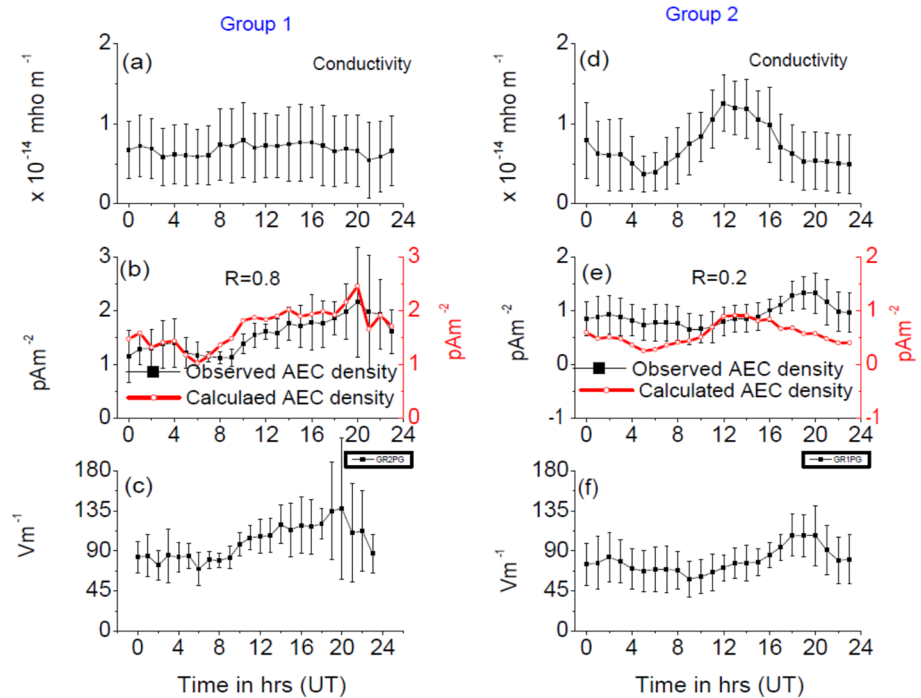


Figure 9. Mean diurnal variation of various atmospheric electricity parameters in summer. Group 1 (shown in the left panel) corresponds to days when the conductivity variation is nearly constant; while, Group 2 (shown in the right panel) represents the days when strong diurnal variability is seen. (a) and (d) Mean diurnal variation of the total conductivity for Group 1 and 2, (b) and (e) Same as (a) and (d) but for observed and calculated air-Earth current density. (c) and (f) Same as (a) and (d) but for potential gradient.

5.2. On Selection Criteria and Diurnal Variation

The data selected based on the criteria presented in Section 4.1 shows different diurnal patterns (Figure 6). The diurnal variation patterns for 1, 6, 15, 16, 18, 20, 28, and 29 March 2019 are nearly similar. But, the sky condition and wind speed and direction were different. At the same time, these trends have a deviation from the GRD (i.e., Carnegie type variation) by having a depression between the two peaks. It is observed that the different sky conditions seldom affect the diurnal pattern. Perhaps the clouds have no sufficient electrical Activity to cause disturbances on the surface measurement of the PG. Localized thunderstorms and ESCs, dust storms, precipitation, fog, pollution, wind speed, aerosols, etc. can significantly influence the atmospheric electrical parameters (Imyanitov & Shifrin, 1962; Kamra, 1969a). In the Arctic and Antarctic, thunderstorm occurrence is rare and is attributed to their local meteorology which does not support the formation of ESCs (Turner et al., 2005). As Antarctica is the least urbanized continent compared to the rest of the continents, its environment is free from dust and pollution. Thus, the electrical perturbations, due to these elements, are naturally reduced. Most of the continent is covered by a thick ice sheet which curtails the emanation of radioactivity from the earth's crust. As such, the heating effect of the incoming solar radiation on the crustal surface is greatly reduced which results in weak convection—an important requirement for the formation of electrified clouds. At the periphery of the continent, this incoming energy is mostly utilized in the melting of ice. Naithani and Dutta (1995) reported the presence of mild convection in the summer season but this is not sufficient for electrified cloud formation. Therefore, we believe that the formation of convective clouds, which would produce lightning and ESC, may not be as vigorous as it is in the tropical region. The minimum and maximum values of the electrically quiet days shown in Figure 6 did not exceed 50 Vm⁻¹ and 150 Vm⁻¹ respectively.

Although it is sparse to have the GRD, we found GRD occurrences in a few days (see the line graph for the days 1, 12, and 20 March in Figure 6). These curves appear to bear the key signatures of the UT-dependent variation of the PG. A minimum of the PG at ~0300 UT, which is one of the key signatures of the GRD, is seen. This could probably be the response of the GEC to the global source (thunderstorms and ESCs). Another signature of the GRD viz. the broad maximum following this minimum can also be seen. An important aspect to be reported is the

broad minimum between the two peaks at ~0600 UT and ~1900 UT on many of the days in Figures 6 and 7b. The probable mechanism involved in the development of this signature shall be discussed in the trailing discussions.

5.3. On Seasonal Variation of PG, AEC Density, and Concentration of Air Ions

Global thunderstorm activity shows a minimum at ~0300 UT and a broad maximum between 0800 UT and 2000 UT (Whipple, 1929). In the past, the measurement of the PG on the Carnegie cruises demonstrated such a pattern. The mechanism responsible for this behavior is the apparent traverse of the Sun and its location on continental landmasses (Williams et al., 2002; Williams & Stanfill, 2002). The advantage of the cruise data is that the measurements were made over the ocean where the Earth's surface is not exposed to the free atmosphere through which the turbulent processes are generated are curtailed (Liu & Liang, 2010; Medeiros et al., 2005). The absence of terrestrial radioactivity and anthropogenic activity will further reduce the electrical complexities in the atmosphere. These features favor the homogeneity atmospheric conductivity. This fact is established, Over Antarctica, by a comparative study of the diurnal variations of the global thunderstorms and ESCs contributing to the GEC suggesting that the diurnal features of the PG are prominent at Vostok (Liu et al., 2010). On the contrary, the seasonal variation of the PG at Maitri displays different diurnal characteristics in summer and winter. The most prominent one is that the trend of the PG variation in winter resembles the Carnegie pattern but it is not in the summer season (Jeeva et al., 2016).

The atmospheric electrical conductivity is controlled by the concentration of small ions and their dynamics. If their concentration is consistent the atmospheric electric conductivity will also be consistent. This is the most important and desirable characteristic of the atmosphere for the AEPs to respond to the global electric sources (Deshpande & Kamra, 2001; Ruhnke, 1962). Figures 7c and 7d demonstrates a significant diurnal and seasonal variation of the concentration of bipolar small ions, which obviously, leads to the diurnal and seasonal variation of electrical conductivity to prevent the consistency in the conductivity. Therefore the diurnal variation in the PG (Figure 7b) is more of in situ characteristics, in response to Figure 7d rather than the global. The cause for the diurnal and seasonal variation of concentration of bipolar small ion is being investigated in a separate work. Yet, we presume that the mild convection over the coastal Antarctic region in the summer season might alter the concentration of ions close to the Earth's surface. It is observed that the temperature is well below 0°C during night-time hours in summer (Figure 7f). As the day breaks and the temperature increases, mild convection occurs which can oppose the flow of the charges along the field lines (Naithani & Dutta, 1995). Therefore, their accumulation is terminated which leads to a decrease in their concentration. During the summer, the mild heating of the earth's surface takes place over Maitri and can lead to this diurnal variation of temperature. Therefore, the AEPs are expected to be slightly disturbed owing to the mild convection in summer. However, the temperature is well below 0°C (Figure 7e) in winter as the Sun is below the horizon. Both these persisting low temperatures and the absence of the Sun do not result in disturbances such as the sunrise effect (Hoppel et al., 1986; Marshall et al., 1999). We do not observe a significant level of diurnal variation in the ion concentration in winter (Figure 7c), which is consistent with the idea that the atmosphere is stably stratified and the space charge does not contribute to significant perturbation in the PG and the AEC density to put some limitation on obtaining GRD. Therefore, it is evident, in summer, that there can be excess positive charges, in the size of small ions, close to the earth's surface at night; however, are depleted during the day by mild convective overturn. During the long polar night in the winter season, the electrode layer will persist forever due to the absence of mild convection.

Usually, the disparity between the concentrations of ions and the electrical conductivity is present in Antarctica [as seen in Figures 3, 7c and 7d]. Ruhnke (1962) found that the conductivity originating from negative ions is $\sim 1.70 \times 10^{-14} \Omega^{-1} \text{ m}^{-1}$, and that from positive ions is $\sim 3.30 \times 10^{-14} \Omega^{-1} \text{ m}^{-1}$. The study suggests that the conductivity due to negative ions was more unstable (volatile) than that due to positive ones, and attributed this to some unknown effects that influence the two ions differently. We believe that one or more of these mechanisms can be involved in the production of the negative ions in the near-earth environment: (a) the Lenard effect (Lenard, 1892), (b) the electrostatic interface effect (Dinger and Gunn (1946), and (c) Jumping frost dendrites (Mukherjee et al., 2021). In the Lenard effect, the surrounding air molecules acquire a negative charge when the water droplets collide with each other or with a wet solid to form fine sprays. In the electrostatic interface process, the charge separation takes place during the melting of the ice. In the process, air acquires either zero or negative charges, and meltwater with either zero or positive charges. The jumping frost dendrites effect is common when the micrometric frost growing on a chilled surface can fracture and jump into the air in the presence of polarizable

liquids. It depends upon the temperature gradient-induced charge separation. In this process, the negative ions are released into the air. We have no intention to look into the details of the sources at this moment. However, we plan to take up a special study on this subject in the future as it involves a few more complementary experiments including ion spectrometer and radiation measurements. The concentration is maximum when the wind is minimum during day hours (see Figure 6f). We interpret this from three different points of view (a) there is a possibility of accumulation of the radioactive gases close to the earth's surface that can enhance the ionization (b) the mechanical force of the wind speed can disperse the concentration of ions, and (c) the wind blowing from the polar plateau is not expected to have radioactive gases (Lockhart et al., 1966). Therefore the concentration of ions is expected to be low when wind speed is high and vice versa.

5.4. Usefulness of Newly Defined Selection Criteria on GRD

Figure 8a clearly shows that the shape of the diurnal curve has a closer resemblance with the Carnegie curve than that seen in Figure 7a. As such, the GRD is reflected better in data that is selected based on the conductivity as an additional criterion than that using fair-weather days. Figure 8b shows that the observed and calculated AEC density significantly co-vary with a correlation coefficient of ~ 0.99 (significance of $P < 1 \times 10^{-4}$). According to Dolezalek (1960), the observed current density is global in nature if it shows a good correlation with the calculated current density, and this can happen only when the electrical conductivity is constant. This result demonstrates that uniform conductivity prevailing throughout the day ensures the detection of global features in PG and AEC density. Generally, the criteria for a fair-weather day that has been used are carefully defined to discard the days linked with any electrical instability due to meteorological processes (Deshpande & Kamra, 2001; Ruhnke, 1962). This method allows eliminating the data affected by processes like precipitation, thunderclouds, drifting snow or dust, fog, etc. but does not guarantee the elimination of the invisible electrical perturbations in the atmosphere, such as aerosol loading and convective activity. We infer that the conductivity measurement is essential to ascertain the complete fair-weather electrical environment and can be annexed to the set of criteria suggested by Burns et al. (2012) as conditions for GRD.

AEC is the sum of the conduction current, convection current, and displacement current. Conduction current is driven by the GEC; while, convection, and displacement current are locally produced. Ideally, the convection current and displacement current should be zero over a site where the conduction current is to be measured. Under this condition, the measured AEC can be assumed to represent the conduction current. An important requirement for this is that there should not be any convective activity on that particular day or location, and the displacement current can be nullified through a condition when there is no variability in the conductivity (Kasemir, 1955). The presence of the conduction current (or the absence of the convection current and displacement current) in the observed AEC is verified by applying atmospheric Ohm's law ($J_c = \sigma TE$) where J_c is the conduction current density, σT is the total conductivity and E represents the PG (Dolezalek, 1960). We find that this condition is fulfilled on the Group 1 day when the atmospheric conductivity has a quasi-flat response over a day.

The poor correlation observed for Group 2 indicates that the observed current density might have a significant contribution from atmospheric fair-weather electrical agitation. The agitations are termed short-term variations of electrical PG (Kamra, 1969b) and the same can be seen in the current also. We suggest that it may arise due to any of the following; (a) the passing of clouds above the observation site, (b) the gusts of wind that perturbs the concentration of aerosols, and (c) the transport of the space charge by convective processes. When the AEP obey Ohm's law the calculated AEC density and observed AEC density are expected to co-vary as there are no variations or fluctuations in the conductivity (Figure 9b). On the contrary, these two curves will be different when the AEPs do not obey Ohm's law due to significant levels of variations or fluctuations in the conductivity (Figure 9c). As we selected the data pertaining to electrically quiet days the first two reasons can be ruled out in the present case. However, the transport of charges/ions by mild convection during summer is possible and can lead to an electrical displacement current. The presence of excess ions of one sign (negative and positive ions in the daytime and night-time, respectively, in the summer season, and the positive ions throughout 24 hr in the long polar night) and their variability is evidence for the displacement. However, in the winter season, there is no significant variation in the concentration of the bipolar ions. As shown in Figures 9c–9f, a comparison of PG variations suggests that the influence of the Asian and African thunderstorm/lightning activity (at 1000 UT and 1600 UT) is significantly weakened for Group 2. Furthermore, the PG variation for Group 1 shows nearly a flat response during 0000 UT - 0600 UT and is in very good agreement with that reported by Torreson

et al. (1946) in this season, in favor of globally representative data. They compared the diurnal variation of the PG for three-month periods from the observations on board the Carnegie, 1915–1921, and 1928–1929. One can see a fairly good agreement among those curves. During May–June–July of 1915–1921, the mean curve invariably shows a secondary peak at ~0800 UT pertaining to the peak thunderstorm activity over Asia. However, this peak is weak during Nov–Dec–Jan of 1928–1929. Possibly the weak thunderstorm and ESC activity over Asia in the Northern Hemisphere winter led to such behavior.

5.5. Historical Support

The present study shows a strong similarity with the pioneering work of Sir George Simpson (Simpson, 1905) carried out a century ago at the Lapp village of Karasjok (69°17', 25°35'E, 129 m above mean sea level). Simpson (1905) reported five different types of the mean curve for the PG variations for the whole year, winter, spring, summer, and autumn. His diurnal curve in winter shows a minimum at ~0400 UT, followed by a steady increase, and a maximum between 1700 UT and 1900 UT (similar to the well-known Carnegie curve). His curves show greater global representativeness in local winter than in the other seasons. In his time, global thunderstorm activity and ESCs were not conceptualized, and the diurnal variation of the PG was discussed in terms of the variation of meteorological weather parameters, ionization, and dissipation. His curve in summer shows a minimum of ~0400 UT but a broad depression between 0800 UT and 1900 UT which is also seen in the present study for Group 2. The measurements of the PG at Potsdam during the period 1904–1923 also reveal the same features (Israel, 1973). Supported by these pioneering studies, we conclude that the winter season has better scope for the PG to bear the signatures of the global thunderstorms and ESCs, irrespective of the hemisphere. Continuous darkness, or the Sun at lower elevations in winter, suppresses convective overturn which in turn stabilizes the atmosphere, thereby, making electrical medium (characterized by electrical conductivity) more stable. Further, the role of the PBL in winter is somewhat similar to that of the Ocean surface where neither radioactive emanation nor convection occurs. Overall, these suppress local fluctuations to deliver a more smoothly varying globally representative signal.

6. Conclusions

The majority of studies on AEPs from the Antarctic continent address either the PG or AEC density measurements or both (Bering et al., 1991; Burns et al., 1995, 2017; Byrne et al., 1993; Cobb, 1977; Frank-Kamenetsky et al., 2001). We investigated for the first time the role of the bipolar ions concentration/conductivity in defining the GRD. Simultaneous measurements of PG and AEC density along with the bipolar ion concentration/conductivity were carried out at Maitri in 2019. Salient features of the present study are as follows:

An important selection criterion for determining fair-weather days is clear-sky (with less than 3-octa high clouds) observations (Deshpande & Kamra, 2001; Ruhnke, 1962). An examination of data for different cloud coverage and wind speed conditions shows that GRD can exist even on cloudy sky days. As the majority of the continent is covered by ice sheets and experiences very low incoming solar radiations sufficient convection might not take place to produce electrified clouds. This feature enabled us to increase the percentage of qualifying data, supported by Burns et al. (2012), significantly. Therefore, on cloudy days with more than 3 octa, the actual electrical disturbances need to be ascertained based on the fluctuation patterns and distribution of the concentration of ions in the air.

Fair-weather days based on standard selection criteria (Burns et al., 2012; Deshpande & Kamra, 2001; Ruhnke, 1962) do not always yield the GRD over Maitri. We found that the level of conductivity variation greatly defines the possibility of GRD. We observed that PG and AEC density are more influenced by local conductivity variations than by the global thunderstorm and ESC activity. This interference is very intense during summer. We recommend the following procedures to obtain the electrically quiet days followed by GRD;

1. One-minute averaged data is suitable to discard the undesirable data rather than the hourly data.
2. A day having strong and rapid fluctuations, exceeding 350 Vm^{-1} , for more than half of a day is rejected. These days are referred very noisy days (e.g., 5 June 2019 in Figure 5)
3. A day having a sudden increase or decrease in PG value, less than ~20%, with respect to the value, throughout the day, may be considered as qualifying data for analysis. They are referred to as electrically quiet days (26 June 2019, Figure 5). On a day if there are fluctuations of data of >20%, for about 4 hr, continuously

or intermittently, data pertaining to that disturbed period may be discarded and the remaining data may be considered for analysis. This type of day is referred to as moderately disturbed data (27 July 2019 in Figure 5).

4. The mean daily PG value should be between 50 Vm^{-1} and 150 Vm^{-1} .
 5. The mean total conductivity should lie between $0.5 \times 10^{-14} \text{ } \Omega^{-1}$ and $0.7 \times 10^{-14} \text{ } \Omega \text{ m}^{-1}$. The desirable range is $0.2 \times 10^{-14} \text{ } \Omega^{-1}$. These criteria will be very useful in the selection of qualifying data from big data sets for analysis. In short the standard deviation of the total conductivity, for the GRD, is recommended to be ~ 0.07 .
 6. The standard deviation of the total conductivity, for the GRD, is recommended to be ~ 0.07 .
1. The seasonal variation of the concentration of small ions shows a strong diurnal variation in summer; however, in winter, this quantity is fairly constant. A detailed investigation is recommended to examine whether any of them or all of the following three processes are involved in the production of excess ions; (a) the Lenard effect (b) the electrostatic interface effect and (c) the Jumping frost dendrites. We believe that the PBL processes can contribute to altering the ion concentration. When a strong diurnal variation of conductivity is present, AEPs are more sensitive to the PBL processes than to the global signals. We found that the absence of the PBL processes stabilizes their concentration in winter which results in fairly uniform conductivity throughout the day. This, in turn, favors the global representation of AEPs in winter. A similar situation is seen in summer when the conductivity remains fairly constant.
 2. Selection of the GRD based on the similarity with the Carnegie curve might often lead to misconception as is observed over Maitri. Therefore, one has to be very careful to distinguish the GRD from the electrically quiet day PG and AEC density curves. The best method to discern the GRD is to establish the stability on account of the electrical conductivity.

We conclude that the diurnal fluctuations in the concentration of ions and electrical conductivity in the summer season are the key issues that mask the global features of the PG and the AEC density. Therefore ion concentration measurements along with the PG and AEC density can immensely contribute to identifying GRD.

Data Availability Statement

Data used in the present study forms part of global electric circuit (GEC) experiments at Maitri, Antarctica, and are available from <https://zenodo.org/record/7824192#ZDeEJnZByUk> and www.iigm.res.in. Plots were created using Origin software.

Acknowledgments

We thank the Directors of the National Centre for Polar and Antarctic Research, Goa, and the Indian Institute of Geomagnetism (IIG), Mumbai, for their constant support in carrying out the studies at Maitri, Antarctica. Thanks are due to Mr. Gopalakrishnan, Mr. Manoj, Mr. Selvaraj, and Mr. Venkatesh for their support in providing the engineering support in designing the electrometers. We thank Dr. S. Sathish Kumar for his continued support as and when required. The authors thank Dr. Navin Parihar for his support in editing the manuscript. The authors express their sincere gratitude to the India Meteorological Department for providing data to verify the AWS operated by IIG. One of the authors (A.K.K.) acknowledges the support of the INSA Honorary Scientist program. We are thankful to the anonymous reviewer for pointing out various critical points to improve the manuscript.

References

- Bering, E. A., III, Benbrook, J. R., Byrne, G. J., & Few, A. A. (1991). Measurements of vertical atmospheric electric current at a network of sites in Antarctica including manned stations & automatic geophysical observations. In S. Michnowski & L. H. Ruhnke (Eds.), *Proceedings of the international workshop on global atmospheric electricity measurements* (Vol. 238, pp. 119–135). Publications of the Institute of Geophysics, Polish Academy of Sciences D-35.
- Burns, G. B., Frank-Kamenetsky, A. V., Tinsley, B. A., French, W. J., Griogioni, P., Camporeale, G., & Bering, E. A. (2017). Atmospheric global circuit variations from Vostok and Concordia electric field measurements. *American Meteorological Society*, *74*(3), 783–800. <https://doi.org/10.1175/JAS-D-16-0159.1>
- Burns, G. B., Frank-Kamenetsky, A. V., Troshichev, O. A., Bering, E. A., & Reddell, B. D. (2005). Interannual consistency of bi-monthly differences in diurnal variations of the ground-level, vertical electric field. *Journal of Geophysical Research*, *110*(D10), D10106. <https://doi.org/10.1029/2004JD005469>
- Burns, G. B., Hesse, M. H., Parcell, S. K., Malachowski, S., & Cole, K. D. (1995). The geoelectric field at Davis station, Antarctica. *Journal of Atmospheric and Terrestrial Physics*, *57*(14), 1783–1797. [https://doi.org/10.1016/0021-9169\(95\)00098-M](https://doi.org/10.1016/0021-9169(95)00098-M)
- Burns, G. B., Tinsley, B. A., Frank-Kamenetsky, A. V., Troshichev, O. A., French, W. J. R., & Klekociuk, A. R. (2012). Monthly diurnal global atmospheric circuit estimates derived from Vostok electric field measurements adjusted for local meteorological & solar wind influences. *Journal of the Atmospheric Sciences*, *69*(6), 2061–2082. <https://doi.org/10.1175/JAS-D-11-0212.1>
- Byrne, G. J., Benbrook, J. R., Bering, E. A., Few, A. A., Morris, G. A., Trabucco, W. J., & Paschal, E. W. (1993). Ground-based instrumentation for measurements of atmospheric conduction current and electric field at the south pole. *Journal of Geophysics*, *98*(D2), 2611–2618. <https://doi.org/10.1029/92JD02303>
- Chalmers, J. A. (1957). *Atmospheric electricity* (2nd ed.). Pergamon Press Ltd.
- Cobb, W. E. (1977). Atmospheric electric measurements at the South Pole. In H. Dolezalek & R. Reiter (Eds.), *Electrical processes in atmospheres* (pp. 161–167). Dr. Dietrich Steinkopff Verlag.
- Deshpande, C. G., & Kamra, A. K. (2001). Diurnal variations of the atmospheric electric field and conductivity at Maitri, Antarctica. *Journal of Geophysical Research*, *106*(D13), 14207–14218. <https://doi.org/10.1029/2000JD900675>
- Dhanorkar, S. S., Deshpande, C. G., & Kamra, A. K. (1989). Observations of some atmospheric electrical parameters in the surface layer. *Atmospheric Environment*, *23*(4), 839–841. [https://doi.org/10.1016/0004-6981\(89\)90488-5](https://doi.org/10.1016/0004-6981(89)90488-5)
- Dinger, J. E., & Gunn, R. (1946). Electrical effects associated with a change of state of water. *Terrestrial Magnetism and Atmospheric Electricity*, *51*(4), 477. [https://doi.org/10.1016/0004-6981\(89\)90488-5](https://doi.org/10.1016/0004-6981(89)90488-5)

- Dirscherl, M. C., Dietz, A. J., & Kuenzer, C. (2021). Seasonal evolution of Antarctic supraglacial lakes in 2015–2021 and links to environmental controls. *The Cryosphere*. <https://doi.org/10.5194/tc-2021-203>
- Dolezal, H. (1960). Zur Berechnung des luftelektrischen Stromkreises III Kontrolle des Ohmschen Gesetzes durch Messung. *Geophysica applicata*, 46(1), 125–144. <https://doi.org/10.1007/bf02001103>
- Frank-Kamenetsky, A. V., Troshichev, O., ABurns, G. B., & Papitashvili, V. O. (2001). Variations of the atmospheric electric field in the near pole region related to the interplanetary magnetic field. *Journal of Geophysical Research*, 106(A1), 179–190. <https://doi.org/10.1029/2000JA900058>
- Gajananda, K., Kaushik, A. N., & Dutta, H. N. (2004). Thermal convection over East Antarctica: Potential microorganism dispersal. *Aerobiologia*, 20(1), 21–34. <https://doi.org/10.1023/B:AERO.0000022987.57564.20>
- Harrison, R. G. (2013). The Carnegie curve. *Surveys in Geophysics*, 34(2), 209–232. <https://doi.org/10.1007/s10712-012-9210-2>
- Hoppel, W. A., Anderson, R. V., & Willett, J. C. (1986). Atmospheric electricity in the planetary boundary layer. In *Study in geophysics—The Earth's electrical environment* (pp. 149–165). National Academy Press. Retrieved from <https://www.nationalacademies.org/legal/privacy>
- Imyanitov, I. M., & Shifrin, K. S. (1962). Present state of research on atmospheric electricity. *Soviet Physics - Uspekhi*, 5(2), 292–322. <https://doi.org/10.1070/PU1962v005n02ABEH003413>
- Israel, H. (1957). Atmospheric electric and meteorological investigations in high mountain ranges. Final report, Air Research and Development Command, ISAF, Contract AF 61 (514)–640.
- Israel, H. (1970). *Fundamentals, conductivity, and ions*. In *Atmospheric electricity* (Vol. I). Israel Program For Scientific Translations.
- Israel, H. (1973). *Fields, charges, currents* (Vol. II, p. 351). Atmospheric Electricity, Israel Program for Scientific Translation.
- Jeeva, K., Gurubaran, S., Williams, E. R., Kamra, A. K., Sinha, A. K., Guha, A., et al. (2016). Anomalous diurnal variation of atmospheric potential gradient and air-Earth current density observed at Maitri, Antarctica. *Journal of Geophysical Research*, 121(12), 593–12611. <https://doi.org/10.1002/2016JD025043>
- Jeeva, K., Panneerselvam, C., Nair, K. U., Selvaraj, C., Dhar, A., Pathan, B. M., & Gurubaran, S. (2011). Global electric circuit parameters and their variability observed over Maitri, Antarctica. *Journal of the Geological Society of India*, 78(3), 199–210. <https://doi.org/10.1007/s12594-011-0088-2>
- Jeeva, K., Seemala, G. K., Selvaraj, C., Rathod, G., Kamra, A. K., & Sinha, A. K. (2021). Responses of various types of antennas to the globally distributed air-Earth current monitored at Maitri, Antarctica. *Polar Science*, 30, 100657. <https://doi.org/10.1016/j.polar.2021.100657>
- Kamra, A. K. (1969a). Effect of wind on diurnal and seasonal variations of atmospheric electric field. *Journal of Geophysical Research*, 31(10), 1281–1286. [https://doi.org/10.1016/0021-9169\(69\)90024-5](https://doi.org/10.1016/0021-9169(69)90024-5)
- Kamra, A. K. (1969b). Short-term variations in atmospheric electric potential gradient. *Journal of Atmospheric and Terrestrial Physics*, 31(10), 1273–1279. [https://doi.org/10.1016/0021-9169\(69\)90023-3](https://doi.org/10.1016/0021-9169(69)90023-3)
- Kasemir, H. W. (1955). *Measurement of air-Earth current density: Proceedings of conference on atmospheric electricity*. *Geophysical Research Paper No. 42* (pp. 91–95). Air Force Cambridge Research Center.
- King, J. C., & Turner, J. (1997). Physical climatology. In *Antarctic meteorology & climatology* (pp. 61–141). Cambridge University Press.
- Kumar, A., Gupta, V. B., Dutta, H. N., & Ghude, S. D. (2007). Mathematical modelling of katabatic winds over Schirmacher region, East Antarctica. *IGRSP*, 36, 204–212.
- Lenard, P. (1892). Über die Electricität der Wasserfälle. *Annalen der Physik und Chemie*, 282(8), 584–586. <https://doi.org/10.1002/andp.18922820805>
- Liu, C., Williams, E. R., Zipser, E. J., & Burns, G. B. (2010). Diurnal variations of global thunderstorms & electrified shower clouds and their contribution to the global electric circuit. *Journal of the Atmospheric Sciences*, 67(2), 309–323. <https://doi.org/10.1175/2009JAS3248.1>
- Liu, S., & Liang, X. Z. (2010). Observed diurnal cycle climatology of planetary boundary layer height. *Journal of Climate*, 23(21), 5790–5809. <https://doi.org/10.1175/2010JCLI3552.1>
- Lockhart, L. B., Patterson, R. L., & Saunders, A. W. (1966). Airborne radioactivity in Antarctica. *Journal of Geophysical Research*, 71(8), 1985–1991. <https://doi.org/10.1029/jz071i008p01985>
- Lutgens, F. K., & Tarbuck, E. J. (2001). *The atmosphere* (8 ed., p. 484). Prentice Hall.
- Mac Gorman, D. R., & Rust, W. D. (1998). *The electrical nature of storms*. Oxford University Press.
- Marshall, T. C., Rust, W. D., Stolzenburg, M., Roeder, W. P., & Krehbiel, P. R. (1999). A study of enhanced fair-weather electric fields occurring soon after sunrise. *Journal of Geophysical Research: Atmospheres*, 104(D20), 24455–24469. <https://doi.org/10.1029/1999JD900418>
- Medeiros, B., Hall, A., & Stevens, B. (2005). What controls the mean depth of the PBL? *Journal of Climate*, 18(16), 3157–3172. <https://doi.org/10.1175/JCLI3417.1>
- Minamoto, Y., & Kadokura, A. (2011). Extracting fair-weather data from atmospheric electric-field observations at Syowa Station, Antarctica. *Policy Sciences*, 5(3), 313–318. <https://doi.org/10.1916/j.polar.2011.07.001>
- Mukherjee, R., Ahmadi, S. F., Zhang, H., Qiao, R., & Boreyko, J. B. (2021). Electrostatic jumping of frost. *ACS Nano*, 15(3), 4669–4677. <https://doi.org/10.1021/acsnano.0c09153>
- Nagaraja, K., Prasad, B. S. N., Madhava, M. S., Chandrashekar, M. S., Paramesh, L., Sannappa, J., et al. (2003). Radon and its short-lived progeny: Variations near the ground. *Radiation Measurements*, 36(1–6), 413–417. [https://doi.org/10.1016/S1350-4487\(03\)00162-8](https://doi.org/10.1016/S1350-4487(03)00162-8)
- Naithani, J., & Dutta, H. N. (1995). Acoustic sounder measurements of the planetary boundary layer at Maitri, Antarctica. *Boundary-Layer Meteorology*, 76(1–2), 199–207. <https://doi.org/10.1007/BF00710897>
- Nicoll, K. A., Harrison, R. G., Barta, V., Bor, J., Brugge, R., Chillingarian, A., et al. (2019). A global atmospheric electricity monitoring network for climate and geophysical research. *Journal of Atmospheric and Solar-Terrestrial Physics*, 184, 18–29. <https://doi.org/10.1016/j.jastp.2019.01.003>
- Price, C., & Rind, D. (1992). A simple lightning parameterization for calculating global lightning distributions. *Journal of Geophysical Research*, 97(D9), 9919–9933. <https://doi.org/10.1029/98JD02651>
- Price, C., & Rind, D. (1993). What determines the cloud-to-ground lightning fraction in thunderstorms. *Geophysical Research Letters*, 20(6), 463–466. <https://doi.org/10.1029/93GL00226>
- Ramesh, K. J., & Soni, V. K. (2018). Perspectives of Antarctic weather monitoring and research efforts. *Polar Science*, 18, 183–188. <https://doi.org/10.1016/j.polar.2018.04.005>
- Ravindra, R., Chaturvedi, A., & Beg, M. J. (2004). Meltwater lakes of Schirmacher Oasis—their genetic aspects and classification. In P. Sahoo (Ed.), *Advances in marine and antarctic sciences*.
- Reddell, B. D., Benbrook, J. R., & Bearing, E. A. (2004). Seasonal variations of atmospheric electricity measured at Amundsen-Scott South Pole Station. *Journal of Geophysical Research*, 109(A9), A09308. <https://doi.org/10.1029/2004JA010536>
- Ruhnke, L. H. (1962). Electrical conductivity of air on the Greenland ice cap. *Journal of Geophysical Research*, 67(7), 2767–2772. <https://doi.org/10.1029/JZ067i007p02767>
- Simpson, G. C. (1905). Atmospheric electricity in high latitudes. *Philosophical Transactions*, 205, 6197.

- Tacza, A., Nicoll, K. A., Macotela, E. L., Kubicki, M., Odzimek, A. M., & Manninen, J. (2021). Measuring global signals in the potential gradient at high latitude sites. *Frontiers of Earth Science*, 8. <https://doi.org/10.3389/feart.2020.614639>. ISSN 2296-6463
- Torreson, O. W., Parkinson, W. C., Gish, O. H., & Wait, G. R. (1946). *Ocean atmospheric electricity results, scientific results of Cruise VII of the Carnegie during 1928–1929*. Publ. 568. Carnegie Institute, Washington, D.C. U.S. Department of Commerce, National Oceanic and Atmospheric Administration, National Geophysical Data Center, 2006. 2-minute Gridded Global Relief Data (ETOPO2v2), 2007. Retrieved from <http://www.ngdc.noaa.gov/mgg/fliers/06mgg01.html>
- Turner, J., Colwell, S. R., Marshall, J., Lachlan–Cope, T., Carleton, A. M., Jones, P. D., et al. (2005). Antarctic climate change during the last 50 years. *International Journal of Climatology*, 25(3), 279–294. <https://doi.org/10.1002/joc.1130>
- Wang, H., Wang, B., Niu, X., Song, Q., Li, M., Luo, Y., et al. (2020). Study on the change of negative air ion concentration and its influencing factors at different spatio-temporal scales. *Global Ecology, and Conservation*, 23, e01008. <https://doi.org/10.1016/j.gecco.2020.e01008>
- Whipple, F. J. W. (1929). On the association of the diurnal variation of the electric potential gradient in fine weather with the distribution of thunderstorms over the globe Q. *J. R. Meteorol. Soc.*, 55(229), 1–18. <https://doi.org/10.1002/qj.49705522902>
- Whipple, F. J. W., & Scrase, F. J. (1936). Point discharge in the electric field of the Earth. *Geophys. Memoirs (London)*, VIII(68), 20.
- Williams, E., Rosenfeld, D., Madden, N., Gerlach, J., Gears, N., Atkinson, L., et al. (2002). Contrasting convective regimes over the Amazon: Implications for cloud electrification. *Journal of Geophysical Research*, 107(D20), 8082. <https://doi.org/10.1029/2001JD000380>. (LBA special Issue, D20, 8082).
- Williams, E., & Stanfill, S. (2002). The physical origin of the land-ocean contrast in lightning activity. *Comptes Rendus Physique*, 3(10), 1277–1292. [https://doi.org/10.1016/S1631-0705\(02\)01407-X](https://doi.org/10.1016/S1631-0705(02)01407-X)